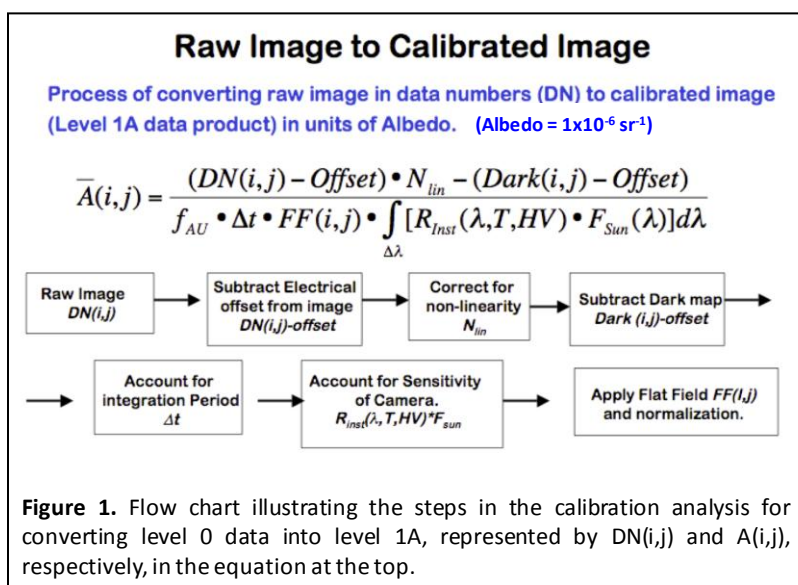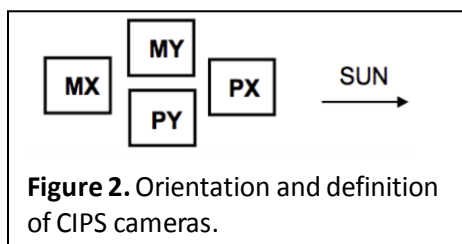# CIPS Calibration
Last Updated 11 December 2011

## 1. Description of Calibration

This document gives a brief overview of the CIPS Level 1A calibration process. For a more detailed description of the CIPS instrument and calibration see McClintock *et al* [2009]. Each image from each camera is calibrated separately, and the resulting calibrated images are stored in the level 1A data product. The calibration process is described by the equation and flowchart depicted in Figure 1. Note that while the fundamental steps of this process never change, some specific methods used to implement the calibration have changed over the CIPS mission in response to changes in measurement sequences and satellite commanding constraints. These changes are noted in the description contained here.



**Raw Image to Calibrated Image**

Process of converting raw image in data numbers (DN) to calibrated image (Level 1A data product) in units of Albedo. (Albedo = $1 \times 10^{-6}$ sr$^{-1}$)

$$\overline{A}(i,j) = \frac{(DN(i,j) - Offset) \bullet N_{lin} - (Dark(i,j) - Offset)}{f_{AU} \bullet \Delta t \bullet FF(i,j) \bullet \int_{\Delta\lambda} [R_{Inst}(\lambda,T,HV) \bullet F_{Sun}(\lambda)]d\lambda}$$

Raw Image $DN(i,j)$ → Subtract Electrical offset from image $DN(i,j)$-offset → Correct for non-linearity $N_{lin}$ → Subtract Dark map $Dark(i,j)$-offset →

→ Account for integration Period $\Delta t$ → Account for Sensitivity of Camera. $R_{inst}(\lambda,T,HV)*F_{sun}$ → Apply Flat Field $FF(I,j)$ and normalization.

**Figure 1.** Flow chart illustrating the steps in the calibration analysis for converting level 0 data into level 1A, represented by DN(i,j) and A(i,j), respectively, in the equation at the top.

The four CIPS cameras are denoted as PX, MX, MY and PY. As diagrammed in Figure 2, the X cameras are aligned fore and aft in the X (along-track) direction, while the nadir Y cameras are aligned in the Y (cross-track) direction (P represents "plus" and M represents "minus" relative to this coordinate system). The AIM satellite is always oriented so that the PX camera is in the sunward direction – in the Northern Hemisphere (NH) this corresponds to the satellite ram direction, whereas in the Southern Hemisphere (SH) the satellite is rotated 180 degrees so that PX is in the anti-ram direction.
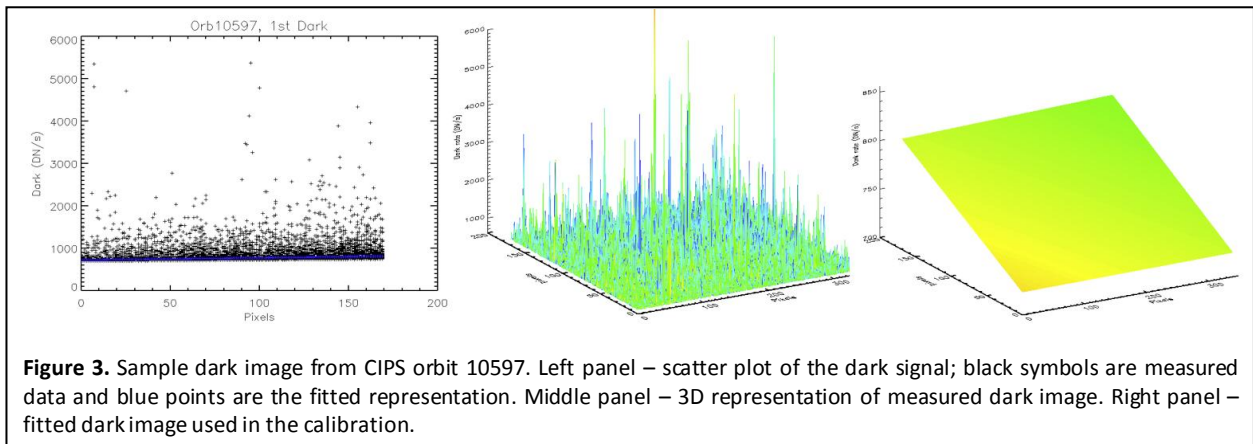


**Figure 2.** Orientation and definition of CIPS cameras.

## 1.1 Dark Correction Maps

The first step in the calibration process is to subtract a dark image from each data image. Prior to 15 September 2011 one dark image (which is taken with the electriconic shutter off) was obtained for each camera at the beginning and end of every third orbit, forming a pair. After this date, the CIPS data sequence was modified to obtain three dark images on every single orbit. To process each science image in an orbit, we first obtain from the Level 0 database a pair of "good" dark images for each camera. To be "good", the pair cannot have missing data packets and must have a valid CCD temperature (obtained from housekeeping data) tagged to the image.

Sometimes one or more of the dark images from a given orbit are noisy (have a higher standard deviation than normal). This can be caused by random particle hits, for example, or by the enhanced radiation environment if the orbit passes through the South Atlantic Anomaly. To avoid propagating dark image noise into the science data, the V4.20 algorithms have implemented a filtering technique to remove this noise. A smooth representation of the dark data is produced by performing a 2D (planar) fit to each image, which captures the magnitude and gradient of the dark image while eliminating the random noise component. This fit is then used to correct for the dark levels in the calibration analysis. Figure 3 shows an example of a relatively noisy dark image from one CIPS orbit, along with the smoothed representation used in the analysis.



**Figure 3.** Sample dark image from CIPS orbit 10597. Left panel – scatter plot of the dark signal; black symbols are measured data and blue points are the fitted representation. Middle panel – 3D representation of measured dark image. Right panel – fitted dark image used in the calibration.

Pre-flight testing of the camera dark characteristics indicated that the electrical offset and dark current are temperature-dependent. Each camera CCD warms from usage, with the final image in an orbit taken at a temperature ~3 degrees warmer than the cold first image. Therefore the dark image pairs, with their associated temperatures, are used to linearly interpolate in temperature to determine an appropriate dark image to subtract from each science image in an orbit.

*Dark image electrical offset correction*

The electrical offset is a baseline signal that is electronically added to each image on-board to avoid a negative readout. The electrical offset is added at the readout register on the CCD. Each dark image electrical offset is calculated using the minimum value from the dark image's first readable row. We subtract this electrical offset from each science image.

*Dark map*

The dark map is defined as the dark image with the electrical offset subtracted from it. The residual dark counts are random in nature, but there is a systematic increase of counts along the axis of the CCD readout direction in the readout register. The additional noise source is due to thermal noise that accumulates as the CCD is read out and is referred to as readout noise. In the image processing the dark offset is subtracted from the dark image to produce a dark map, which is then subtracted from the science image.

**1.2 Non-Linearity**

The "summing well" is the limiting charge collecting structure on the detector CCD. Pre-flight characterizations indicated that the CCD has a non-linear structure when the summing well exceeds the limiting charge. Therefore we apply a non-linearity correction to the observed detector signal ($DN_{Observed}$):

$$DN_{True} = \frac{DN_{Observed}}{1 + \alpha \bullet DN_{Observed}^2}.$$

This relationship is valid for $DN_{Observed} < 1.5 \times 10^4$. The nonlinearity correction is applied to the science image after the electrical offset is subtracted. Values of $\alpha$ for a 4×8 binning for the individual cameras are shown in Table 1.

| Camera | $\alpha$ |
|:---:|:---:|
| PX | $-4.65 \times 10^{-12}$ |
| PY | $-6.28 \times 10^{-12}$ |
| MX | $-6.67 \times 10^{-12}$ |
| MY | $-6.14 \times 10^{-12}$ |

**Table 1.** Nonlinearity coefficients for 4×8 binning

### 1.3 Integration period

The dark map and the science images are divided by the integration period ($\Delta t$ in Equation 1) to produce a unit detector count rate (DN/s). The nominal integration period is 1.024 seconds for the X cameras and 0.714 seconds for the Y cameras. At the same time a correction ($f_{AU}$ in Equation 1) is applied to compensate for the seasonal change in the Earth-Sun distance in normalizing to a standard solar flux.

### 1.4 Camera Radiometric Sensitivity and Micro-Channel Plate (MCP) gain correction

The radiometric sensitivity of each camera was determined in pre-flight testing. The radiometric sensitivity factors convert the detector count rate (DN/s) into albedo units (1 albedo unit = $10^{-6}$ $sr^{-1}$). Table 2 lists the camera radiometric sensitivity factors corresponding to intensifier voltage V=700 volts and a temperature of $22^o$C.

| Camera | 4×8 binning (DN/sec/albedo) |
|:---:|:---:|
| PX | 742.7 |
| MX | 1300.5 |
| PY | 618.7 |
| MY | 596.5 |

**Table 2.** Radiometric sensitivity factors for converting detector signals (DN/s) to albedo units. These factors correspond to lab conditions of V=700 volts, T=$22^o$C.

Preflight testing determined that the MCP gain correction varies with the CCD temperature and the high voltage. A correction of the functional form below was determined from laboratory calculations. The best-fit parameters for each camera are listed in Table 3. Each science image is divided by the radiometric sensitivity correction and multiplied by the MCP gain correction. At this point all images are in albedo units.

$$G(HV, T) = Ao \, (a_3 + a_4 \cdot T) \cdot e^{a_1 \cdot (HV - 700) + a_2 \cdot (HV - 700)^2}$$

$$Ao = (a_3 + 25.0 \cdot a_4)^{-1}$$

| Camera | MCP Gain Coefficients | | Temperature Gain Coefficients | |
|---|---|---|---|---|
| | $a_1$ | $a_2$ | $a_3$ | $a_4$ |
| PX | 0.0161378 | -9.61494e-06 | 1.02859 | -0.00418869 |
| PY | 0.0153218 | -1.02052e-05 | 1.01431 | -0.00450727 |
| MX | 0.0163646 | -9.77719e-06 | 1.02406 | -0.00441509 |
| MY | 0.0149232 | -9.55688e-06 | 1.03924 | -0.00477110 |

**Table 3.** Best-fit parameters for correcting the radiometric gain factors for dependence on detector high voltage and temperature.
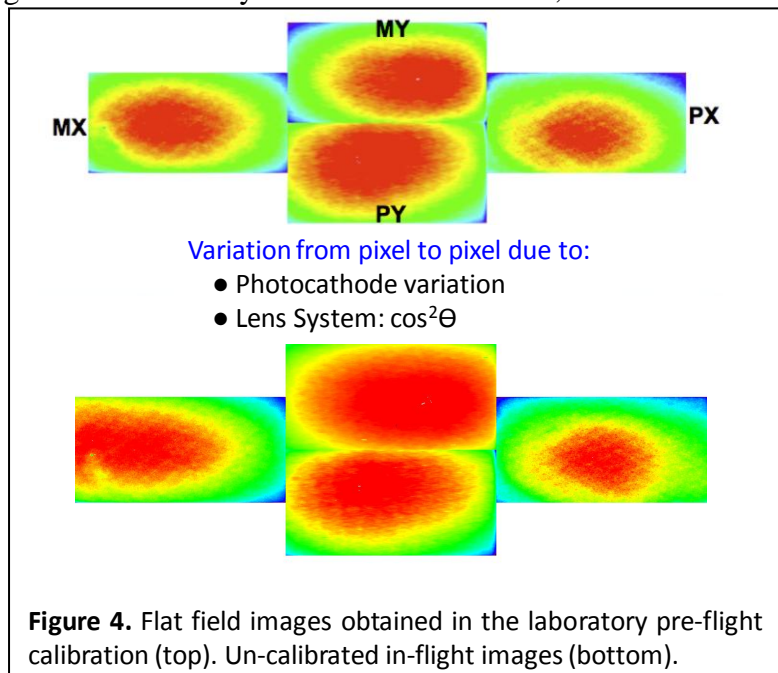
## 1.5 Flat Field correction and camera-to-camera normalization

*Flat Field*

The flat field is the pixel-to-pixel variation of the camera due to the lens system and the photocathode. Each raw camera image is dominated by the flat field variation, as illustrated in Figure 4, which shows both laboratory and non-calibrated flight images for uniform illumination scenes. The non-calibrated scene looks very similar to the lab flat field scene. The flat field variation was mapped out in pre-flight laboratory testing. The variation is normalized to unity in the center of the image, providing a pixel-by-pixel correction factor that is divided out of each science image in the calibration process.

*Delta Flat Field*

The laboratory flat field correction described above should have removed all instrument-induced



**Figure 4.** Flat field images obtained in the laboratory pre-flight calibration (top). Un-calibrated in-flight images (bottom).

pixel-to-pixel variation from the cameras. However when the first on-orbit science images were processed it was evident that there was residual variability across the detector. We refer to this residual as the Delta Flat Field (or Δ-flat for short), as it is a secondary correction to the laboratory flat fielding. This residual non-uniformity must be corrected in the calibration procedure to avoid systematic biases in the CIPS cloud retrievals. The CIPS team has developed additional calibration procedures that make use of special operational datasets obtained on-orbit to characterize and remove this residual variation.

To obtain an accurate estimate of the Δ-flat field we require a uniformly illuminated camera image, a condition that, on orbit, is best realized at the subsolar point in nadir viewing geometry. This scenario has the advantage of minimizing the solar zenith and satellite view angles (thus minimizing scattering angle variation) as well as atmospheric (e.g., ozone) variation across the image. New satellite and instrument commands were devised to obtain CIPS images from each camera at the subsolar point on consecutive orbits at different times during the year. These "special_1a" images are taken either before (SH) or after (NH) the normal science data sequence. The AIM satellite is rotated so that one camera is pointed directly nadir for a series of images, and the sequence is rotated through the four cameras on sequential orbits. These nadir subsolar images are calibrated and then compared to a simulated albedo image calculated from a Rayleigh scattering atmospheric model using the identical viewing geometry (for more details on the model see the level 2 algorithm documentation).

This so-called C/σ Rayleigh model is characterized by two parameters – the ozone column density above a reference altitude (C) and the ratio of the ozone and atmospheric scale heights (σ). Both are assumed constant across the image in the model calculation. The measured subsolar image is then divided by the model image and the resulting ratio is normalized to unity at the image center, to isolate the pixel-to-pixel variation and eliminate any



**Figure 5.** Delta Flat Field images used for the NH 2009 season. Observed patterns in the pixel-to-pixel structure are similar from year to year.

absolute offset between model and data. This process is performed for all subsolar images separately, and the results are averaged to beat down random noise. The result is a final Δ-flat image for each camera for each season, which is then multiplied by each science image at the last stage in the calibration process. The residual variation observed is on the order of 4% for PY, MY and MX and up to 11% for PX, and shows significant structure across the camera. A sample set of Δ-flat images is shown in Figure 5.
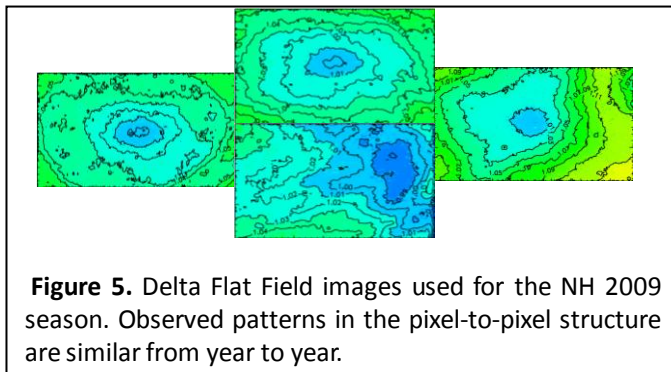
The assumption of constant ozone across the camera field of view in the model calculations necessarily introduces some error into this analysis. Comparison with results from an independent technique based on statistical analysis of overlapping pixels obtained from special fast-cadence images indicates that the operational V4.20 calibration could still have systematic flat field errors up to 1.5% across the cameras (along track direction). While this error seems small, it does affect the retrieval of the dimmest clouds. Because 1.5% of 200 albedo units (a typical background albedo measured by CIPS) is 3 albedo units, the threshold for cloud detection

can vary by 3 albedo units across the detector. This is significant compared to the brightness of the dimmest clouds CIPS detects, which are less than 10 albedo units. We are currently working on new calibration methods with the goal of reducing the systematic flat fielding errors to better than 0.5% in the next CIPS data version.
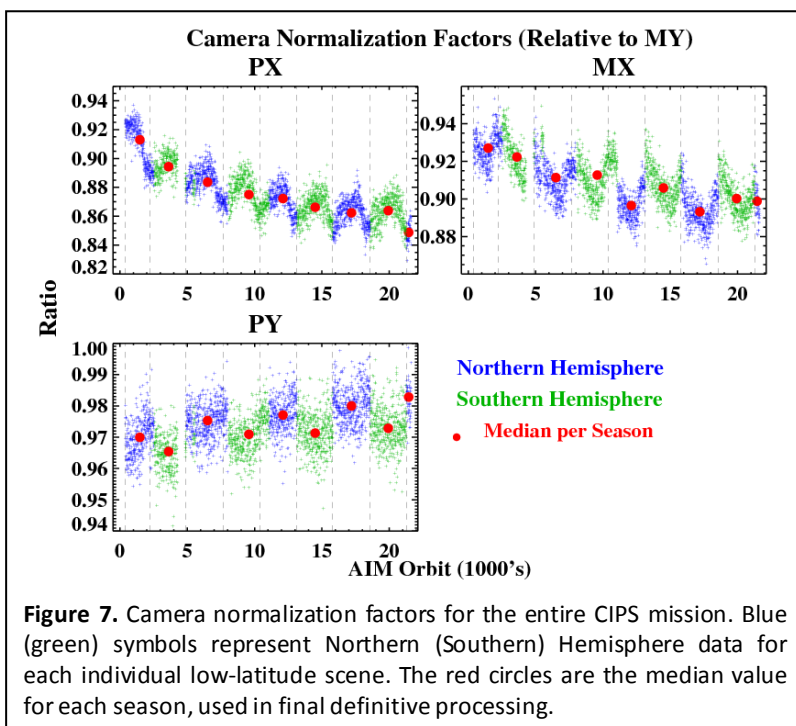
*Camera-to-Camera normalization*
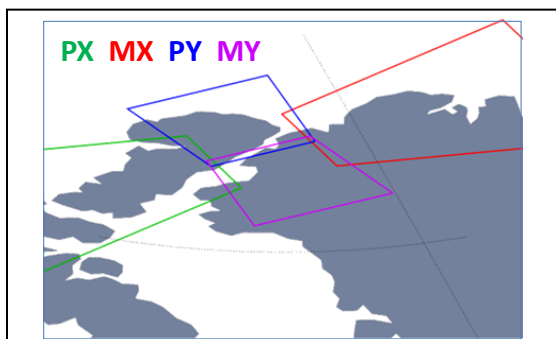


**Figure 6.** CIPS camera footprints at cloud-deck altitude from a typical scene. A CIPS scene consists of images from all four cameras taken simultaneously. Each of the nadir (Y) cameras overlaps all other cameras along some edge pixels, while the PX and MX cameras overlap both Y cameras.

The instantaneous field of view of each camera overlaps that of other cameras as illustrated in Figure 6. The basic CIPS measurement technique involves combining spatially coincident measurements from different cameras, made at different scattering angles, to construct a measured scattering profile (albedo vs. scattering angle). Hence it is critical that the calibration enforce consistent normalization between the cameras. The flat field correction described above is solely concerned with fixing the correct pixel-to-pixel variation across each camera, and thus leaves undetermined an overall calibration constant. The final step of the calibration procedure is then to normalize the relative sensitivity of each camera to the others, which we do by forcing the ratios of observed albedo in these overlapping pixels to be equal. This requires that one camera be used as a standard against which to normalize the others, and the MY camera is chosen because it exhibits the most stable long-term trends.

CIPS measures one extra scene every sixth orbit at low latitudes, outside the normal range of science images where PMCs occur. These images are referred to as "low latitude flats" (LL Flats). Similar to the subsolar images described above, these images are obtained in conditions of relatively uniform illumination and low atmospheric variability. Using this data a normalization factor is obtained for each camera (PX/MX/PY) from each scene by calculating the mean albedo ratio in all overlapping MY pixels. Figure 7 shows these normalization factors over the entire AIM mission to date.



**Figure 7.** Camera normalization factors for the entire CIPS mission. Blue (green) symbols represent Northern (Southern) Hemisphere data for each individual low-latitude scene. The red circles are the median value for each season, used in final definitive processing.

Each vertical line represents a separation of PMC seasons (NH to SH measurements or vice versa). The red circles represent the median normalization in each PMC season and are the factors used in the final calibration process. Obviously this full season average, while always available for reprocessing of past data, is not available for routine operational processing of the current season. For each new season the V4.20 algorithm starts out using Δ-flat and normalization factors obtained from preseason subsolar data, if available. It is sometimes the case that new calibration data has not been obtained before the start of a cloud season, since commanding for these special measurements requires satellite bitlock to uplink commands, and this has been problematic for the AIM mission. In this situation we start operations with the previous year's calibration data (the situation has changed as of September 2011 – please see the discussion that follows). This does not generally present a problem as the Δ-flats are consistent year-to-year. (The normalization factors, as Figure 7 shows, do exhibit trends at the 1-2%/year level, so this is more problematic). At the end of each season we re-calculate a final calibration using all available data and re-process the full season for consistency. Because each season uses a different set of delta flats (defined above) there can be jumps in the normalizations between seasons. We are investigating the decreasing trend of the PX and MX normalizations. In addition, we are investigating the relatively larger discontinuities in the MX and PY normalization in the transition from NH to SH observations.

As of September 2011, due to constraints imposed by loss of satellite bitlock, CIPS is no longer making the "special_1a" subsolar measurements described above. However, the LL Flat images are suitable for use instead of the subsolar images for the purposes of calibration. While the viewing geometry is not as ideal, this data set has the advantage that there are many more images to work with, and they are available continuously throughout the year. This allows us to average many more Δ-flat images to reduce random error, and in principle opens up the possibility for doing time-dependent calibration during a season. Each LL Flat scene provides a self-consistent measurement of both the Δ-flat field for all four cameras, as well as the normalization factors. Also, beginning in September 2011 the CIPS measurement sequence was modified to obtain two LL Flat scenes every orbit, thereby increasing the data density significantly. All CIPS seasons from Southern Hemisphere 2011/2012 and later will use calibration obtained from this data source.

## 2.0 Trends in calibration variables

### 2.1 Dark Trends

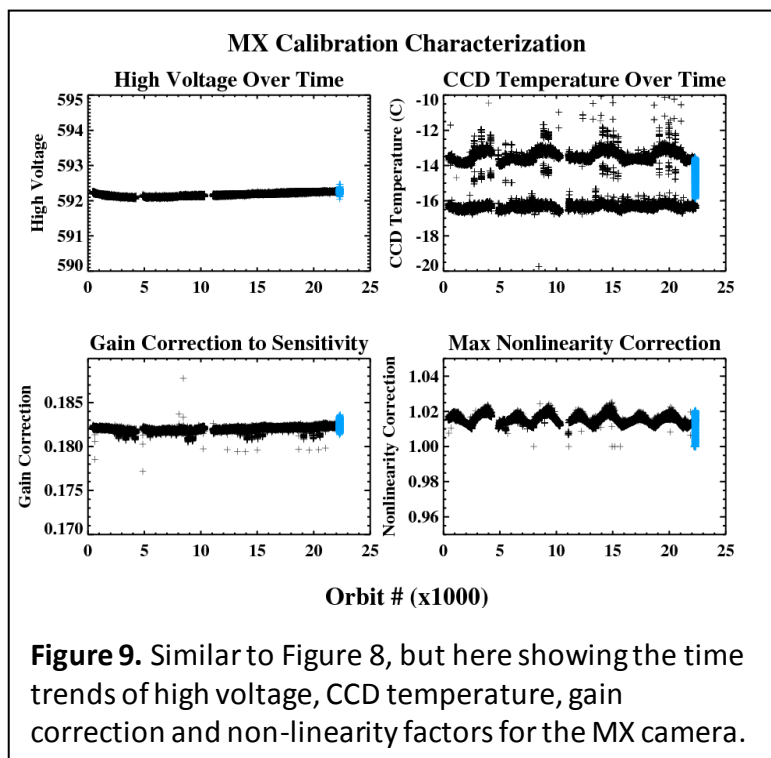Figures 8 and 9 show mission trend plots of variables from the
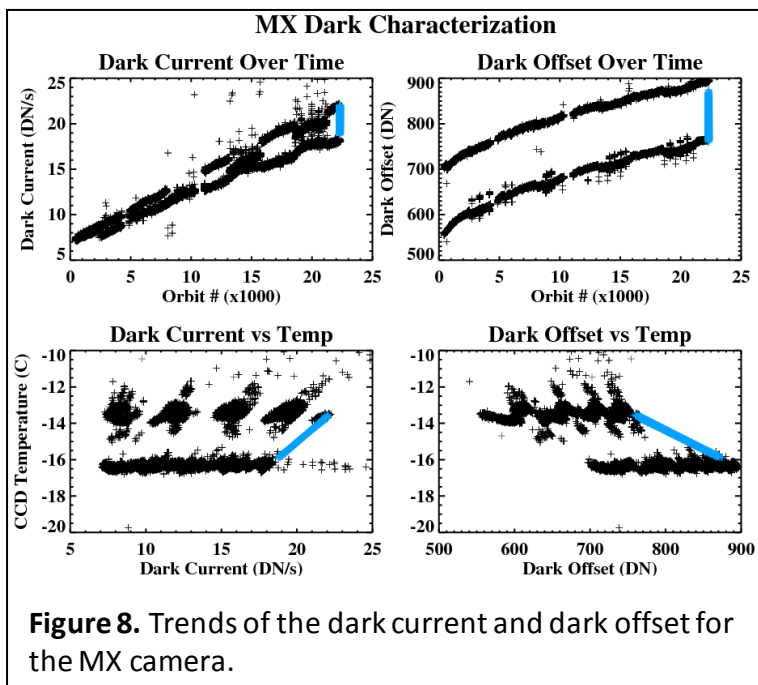


**Figure 8.** Trends of the dark current and dark offset for the MX camera.

7

calibration process. Figure 8 shows trends in the dark current and dark offset from the dark dataset (black data points). The dark datasets, as discussed in section 1.1, are taken for each camera at the beginning and end of every third orbit before September 2011, and every orbit thereafter. Ten dark images per camera were taken each mission day before September 2011and 45 since then. As determined in laboratory measurements, the darks vary with CCD temperature. The CCD temperature warms ~3º over an orbit from usage between the first and last dark images. The two top plots show that the dark current and dark offset for the MX camera increased by ~10% over the mission. The two distinct lines in these plots are due to the dark variation with the CCD temperature. The dark current and dark offset are plotted against CCD temperature in the two bottom figures.

The blue data points represent the temperature-interpolated values from the most recent CIPS data in the time period shown. The dark images taken at the beginning and end of the orbit should bracket the interpolated data. This is a good check to make sure that the darks are interpolated correctly. We only show the MX camera because the other cameras are very similar. Although cameras are getting noisier it seems to be fairly systematic and the camera degradation appears to be very slow. More than four years into the mission the cameras are still very quiet and have good signal to noise.

## 2.2 *Calibration Diagnostics*

Figure 9 shows of the trend of single value calibration diagnostics for the MX camera. These variables are analyzed routinely to determine if the camera is behaving as expected. The High Voltage (per image), CCD temperature (per image), MCP Gain (corrects sensitivity for temperature and high voltage) and Nonlinearity correction are shown. The black points represent the values corresponding to the dark images. The blue points represent science image data from recent orbits. The operational Level 1A processing codes were modified in V4.20 to save out all these critical single value diagnostic variables



**Figure 9.** Similar to Figure 8, but here showing the time trends of high voltage, CCD temperature, gain correction and non-linearity factors for the MX camera.

for every single CIPS image in the Level 1A data files. This makes it much easier than in previous data versions to routinely access these quantities and check for trends and anomalies.

## References

McClintock, William, D.W. Rusch, G.E. Thomas, A.W. Merkel, M.R. Lankton, V.A. Drake, S.M. Bailey, and J.M. Russell III, The Cloud Imaging and Particle Size experiment on the

Aeronomy of Ice in the Mesosphere mission: Instrument concept, design, calibration, and on-orbit performance, J. Atmos. Solar-Terr. Phys., doi:10.1016/j.jastp.2008.10.011, 2009.

Created by Jerry Lumpe and Aimee Merkel, 26 May 2011.
Updated: 11 December 2011 by Jerry Lumpe